ADVANCED OPTICAL MATERIALS
www.advopticalmat.de

Oxide Surface Plasmon Resonance for a New Sensing Platform in the Near-Infrared Range

Hiroaki Matsui, Wasanthamala Badalawa, Akifumi Ikehata, and Hitoshi Tabata*

A new sensor platform is realized by surface plasmon resonance on doped oxide semiconductors of In_2O_3:Sn layers (oxide-based SPR) in the near-infrared range. The detection sensitivity of oxide-based SPR is initially demonstrated by enhancement of the absorption band ascribed to molecular-vibrational modes in the NIR range, which indicates that the enhancing effects occur only when coupling is achieved between excitations of surface plasmons and molecular vibrations. These results are supported by theoretical analyses of electromagnetic field amplitudes on the layer surfaces. Further studies with SPR measurements of glucose-water solutions reveal that the precise detection sensitivity (S) of oxide-based SPR is 7576 nm RIU^{-1}, which is consistent with the theoretically estimated sensitivity (S = 7447 nm RIU^{-1}). The experimentally and theoretically obtained resolution in the refractive index is on the order of 10^{-5}, which also supports the appearance of molecular-vibrational modes in the SPR spectra. Finally, it is found that the detection sensitivity of oxide-based SPR is close to that of Au metal-based SPR working in the visible range, a result that is discussed in relation to the spatial coherence and major characteristics of SP waves at the metal–water interfaces of In_2O_3:Sn and Au layers.

1. Introduction

Oxide plasmonics have received much attention as new phenomena with potential applications because impurity-doping into oxide semiconductors can provide metallic conductivity for the creation of surface plasmon resonances (SPRs). Unlike noble metals such as Ag and Au, plasmon resonance frequencies of doped oxide semiconductors can be tuned by changing the physical parameters of a material, which creates new possibilities for plasmon manipulation of light.[1–3] In particular, the use of SPR devices has become an extremely useful technique to obtain quantitative real-time kinetic information on surface bio-affinity interactions because a slight change of the refractive index of a dielectric on a metal surface can be detected.[4,5] SPR behaviors of doped oxide semiconductors are observed in the near-infrared range owing to a carrier density in the order of 10^{21} cm^{-3}.[3] The NIR range contains anharmonic modes of molecular vibrations (e.g., O–H and C–H), which can be coupled to plasmon resonance. As a consequence, these vibration peaks are markedly enhanced due to the increase of an electromagnetic field on the metal surface caused by the SPR effect.[6,7] This enhancement phenomenon occurs when plasmonic resonance exactly matches the spectral positions of the vibrational fingerprints of molecules.[8] SPR in the NIR range is being applied in biological and chemical fields such as pharmaceutical and medical diagnosis.[9–11] Therefore, oxide-based SPR is expected to open new opportunities for sensing applications in the NIR region.

There are currently many types of oxide semiconductors. However, very few oxide semiconductors are favorable for sensing applications based on SPR because a high electron density (n_e), small effective mass (m^*), and high Hall mobility (μ_H) are required to realize high-performance SPR sensor devices. In contrast, a low n_e, large m^*, and low μ_H provide an increase in conductance losses resulting from high damping of surface plasmons. **Table 1** shows various material parameters of doped oxide semiconductors with metallic conductivity of an *n*-type carrier polarity. Conduction bands (CBs) of In_2O_3 and ZnO are composed of 5s and 4s orbitals, respectively,[12,13] while d orbitals act as conduction paths of electrons in VO_2, TiO_2 and WO_3.[14–16] Oxide semiconductors with CBs of s-orbitals commonly show low m^* and high μ_H values, while high m^* and low μ_H values are characteristic of oxide semiconductors with CBs consisting of d-orbitals. Table 1 showed that In_2O_3:Sn with the 5s-orbital can realize small m^*, high n_e and high μ_H values. In addition, In_2O_3: Sn provides an ideal Drude component in the NIR region because of the absence of interband transitions such as those exhibited by Ag and Au metals. The interband transition of In_2O_3:Sn only shows in the ultra-violet (UV) region. Therefore, this electronic system exhibits the lowest conductance loss in oxide semiconductors in the NIR region, leading to high-performance SPR. Moreover, In_2O_3:Sn is recognized as one of the solid oxide substrates of increasing importance in the area of biosensing and biocompatible materials.

Dr. H. Matsui, Prof. H. Tabata
Department of Bioengineering
The University of Tokyo
1-3-7 Hongo, Bunkyo-ku, Tokyo, 113-8656, Japan
E-mail: hiroaki@ee.t.u-tokyo.ac.jp
Dr. H. Matsui, Dr. W. Badalawa, Prof. H. Tabata
Department of Electronics Engineering and Information systems
1-3-7 Hongo, Bunkyo-ku, Tokyo, 113-8656, Japan
Dr. A. Ikehata
Nondestructive Evaluation Laboratory
Analytical Division, National Food Research Institute
2-1-12 Kannondai, Tsukuba, Ibaraki, 305-8642, Japan.

DOI: 10.1002/adom.201200075

Table 1. Physical properties of metallic oxide semiconductors with electron carriers.

	In_2O_3[a)]	ZnO[b)]	VO_2[c)]	TiO_2[d)]	WO3[e)]
Conduction band	5s	4s	3d	3d	5d
Impurity dopant	Sn^{4+}	Ga^{3+}	W^{5+}	Nb^{5+}	Na^{+}
Carrier density, n_e, [cm^{-3}]	2.0×10^{21}	1.2×10^{21}	3.0×10^{22}	2.9×10^{21}	1.1×10^{22}
Effective mass, m_e^*	0.3 m_o	0.27 m_o	1.6 m_0	1.0 m_o	0.5 m_o
Hall mobility, μ_H, [cm^2/V.s]	42	32	0.1	22	6

[a)]Reference 11; [b)]Reference 12; [c)]Reference 13; [d)]Reference 14; [e)]Reference 15.

The electrical properties of In_2O_3:Sn have been explored to electrically detect immunoanalytes using protein and DNA biomolecules.[17,18] Specifically, biological and chemical reactions between molecules are mainly performed by electrochemical techniques that utilize In_2O_3:Sn layers as transparent surface electrodes.[19–21] Therefore, elucidation of the detection ability of surface plasmon-based sensing that utilizes In_2O_3:Sn allows us to dynamically observe biological and chemical reactions on In_2O_3:Sn layer surfaces at the nano scale, which provides new insight into doped oxide semiconductors as biocompatible materials.

In this work, we explore the potential of oxide-based SPR with In_2O_3:Sn in the NIR region. This paper mainly focuses on two methods in order to determine the detection sensitivity of oxide-based SPR. The first objective is the detection of a slight change of refractive index ascribed to the molecular vibrations of O–H and C–H modes, which demonstrates the resonant interaction between both excitations of plasmon and vibration in the NIR region. The second objective involves experiments with biologically important glucose concentrations in water in order to determine exactly detection the sensitivity of oxide-SPR. Finally, we discuss the spatial coherence and major characteristics of SP waves in order to clarify the spatially sensing region of oxide-SPR in the NIR range. These studies demonstrate the useful potential of oxide-SPR in the NIR range for sensing applications.

2. Surface Plasmons Excited at Water–In_2O_3:Sn Interfaces

Figure 1 shows angle- and wavenumber-dependent SPR absorbance spectra for water at different layer thicknesses (t). SPR was excited using conventional Kretschmann-type attenuated total reflection (ATR). Peaks were not observed with the measurement limit at t = 180 nm (Figure 1a), while SPR peaks clearly appeared in the layers with t = 146, 115, and 107 nm (Figure 1b–d). These peak positions systematically shifted to higher wavenumbers with an increase of θ, as expected for SPR behavior. Since the angle of the incident light modulates the momentum vector, the peak wavenumber of SPR changes along the dispersion curve of SP. On the other hand, for 79 and 63 nm-thick layers, these peak positions gradually shifted from higher to lower wavenumbers with an increase of θ (Figures 1e,f). These phenomena are based on the presence of perpendicularly polarized screened bulk plasmon polaritons (SBPPs), in which the dipole is created by a charge separation across the thin layer.[22] SBPPs can be approximated as dipole plasmons that are distinct from surface plasmon polaritons (SPPs). Detailed information concerning SPP and SBPP modes on doped oxide semiconductors is presented in our previous report in relation to Ga-doped ZnO.[3] The peak positions that resulted from the SPPs and SBPPs of In_2O_3: Sn layers were supported by a theoretical calculation of a multilayer consisting of water, In_2O_3:Sn and BK-7 glass on the basis of the Fresnel reflection model

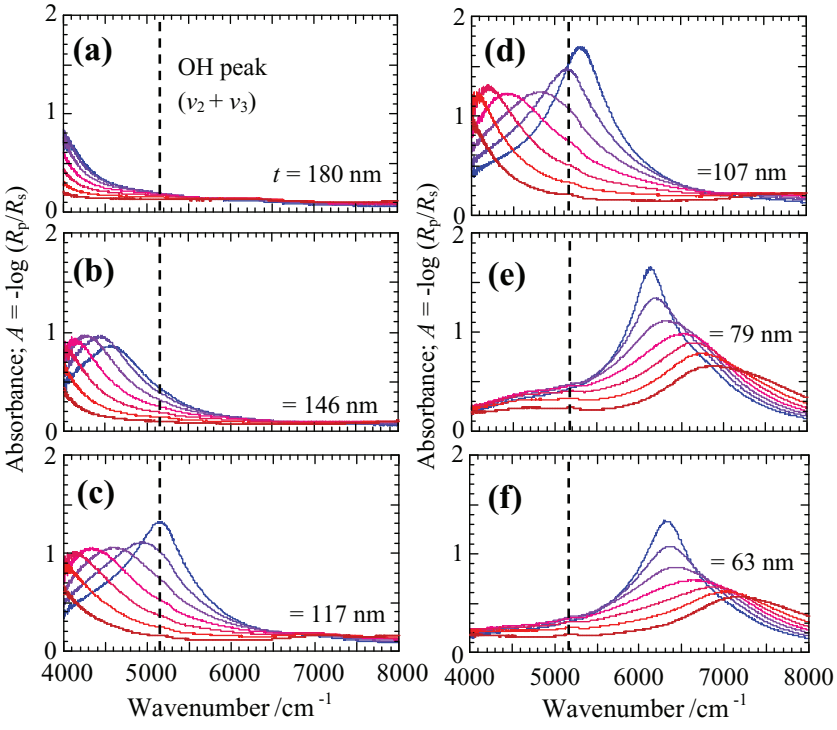

Figure 1. SPR-NIR spectra of In_2O_3:Sn layers with thicknesses of 180 nm (a), 146 nm (b), 115 nm (c), 107 nm (d), 79 nm (e) and 63 nm (f). Water (H_2O) was chosen as the dielectric medium. The incident angle (θ) varies from 64 degrees (red line) to 76 degrees (blue line) in 2-degree increments. The black dotted lines represent the absorption band (OH mode) of water.

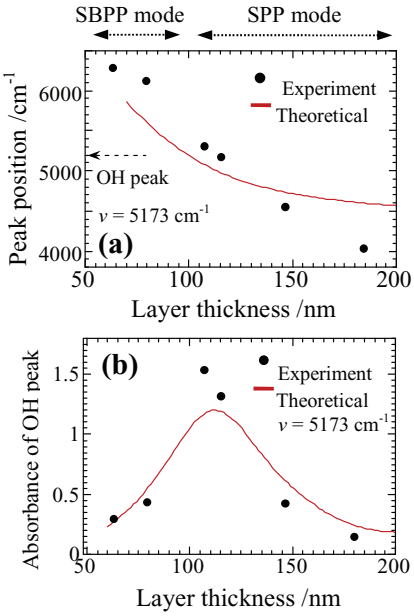

Figure 2. Peak position of experimental SPR spectra with $\theta = 75$ degrees as a function of layer thickness (black dots). The red line was estimated from theoretically calculated SPR spectra. (b) Absorbance of water at 5173 cm^{-1} in experimental SPR spectra as a function of layer thickness (black dots). The red line corresponds to the absorbance of water at 5173 cm^{-1} in theoretically calculated SPR spectra.

(**Figure 2**a and Figure S3). It was found that a layer thickness in the vicinity of 110 nm was required to excite surface plasmons at the In_2O_3:Sn–water interface in the NIR range.

3. Surface Plasmons Coupled with Molecular Vibration Modes

The combination of bending (ν_2) and antisymmetric stretching (ν_3) modes of the water molecular is found at 5173 cm^{-1}.[9] In general, the absorbance of this peak is very small and is less than$A$ = 0.01 (Figure S5b). Figure 1 shows that the combination band ($\nu_2 + \nu_3$) of water at 5173 cm^{-1} was observed in SPR spectra of 115 and 107 nm-thick layers. The absorption of water was enhanced by SPR, especially when the absorption peak of water overlapped with that of SPR (Figure 2a). The highest absorbance of water (A = 1.54) was achieved with SPR using $\theta = 75$ degrees and a 107 nm-thick layer. As a consequence, the intensity of absorption increased by a factor of 10^2 compared with that of attenuated total reflection (ATR), when the peak position of absorption of water overlapped with the peak position of SPR. The increased absorbance of the OH mode in water caused by SPR was evidenced theoretically. We now discuss the enhancement factor (EF) by SPR, which can be expressed by the following equation: $EF = (A_{SPR}|_{\kappa\neq 0} - A_{SPR}|_{\kappa=0})/A_{ATR}$, where $A_{SPR}|_{\kappa\neq 0}$ and $A_{SPR}|_{\kappa=0}$ indicate the absorbance of SPR-NIR spectra of water and that of the reference sample with no absorption band, respectively. The value of κ is the extinction coefficient, and equals 8.62×10^{-4} at 5173 cm^{-1}. It is asumed that $\kappa = 0$ for the reference sample. A_{ATR} indicates the absorbance of ATR. The experimental EF value was 101, which was close to the enhancement factor estimated theoretically (EF = 265).

Absorption-enhanced SPR differs from conventional SPR based on a refractive-index measurement because we measure the absorption using the reflection light that leaks back from the metal layer.[23] If the metal layer is thicker than the penetration depth (δ_m) into the metal layer, the field cannot couple with the radiation light that leaks back from the In_2O_3:Sn layer. The enhancement of water absorption by Au metal-based SPR was observed at a layer thickness of 18.9 nm,[6] which was close to the penetration depth into the Au layer (δ_m = 24.8 nm; see Table 3). On the other hand, the value of δ_m in the In_2O_3:Sn layer was estimated as 115 nm, which theoretically supported the experimental finding of an increased absorbance of water in 115 and 107 nm-thick layers. The theoretical equations for calculating δ_m are presented in Section 9 of the Supporting Information.

Weak optical absorption in a liquid sample on a metal surface is enhanced due to an electromagnetic field caused by SPR at a metal/dielectric interface. In this work, we introduce a quantitative expression that describes the relationship between SPR signals and dielectric constants. This expression is based on the evanescent field treatment, which allows the quantitative analysis of the SPR reflectance of absorbing dielectric media. Therefore, mean-square electromagnetic field distributions were calculated on the basis of the Fresnel formula (Supporting Information, Section 4).[24] **Figure 3**a shows depth profiles of the mean-square evanescent fields of the p-polarized

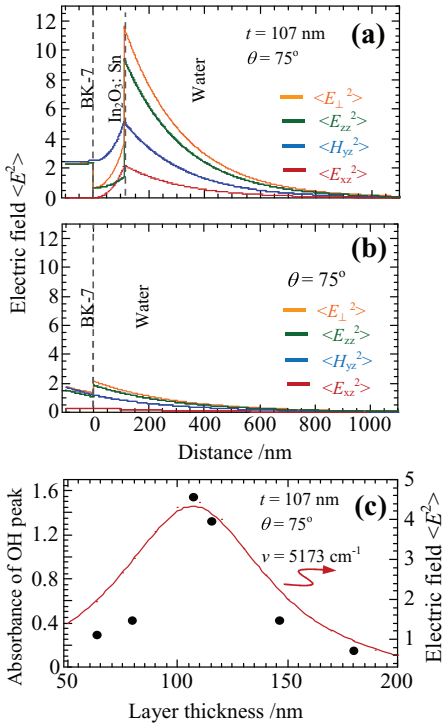

Figure 3. Depth-dependent mean-square evanescent fields of SPR at 5173 cm^{-1}.$\langle H_{yz}^2 \rangle$ represents the mean-square magnetic field. $\langle E_{xz}^2 \rangle$ and $\langle E_{zz}^2 \rangle$ represent the mean square electric fields in the x- andz-directions, respectively. $\langle E_{\perp}^2 \rangle$ indicates the mean-square electric field of parallel (p)-polarized radiation, where $\langle E_{\perp}^2 \rangle = \langle E_{xz}^2 \rangle + \langle E_{zz}^2 \rangle$. The field amplitudes are normalized to the electric field amplitude of the incident radiation.

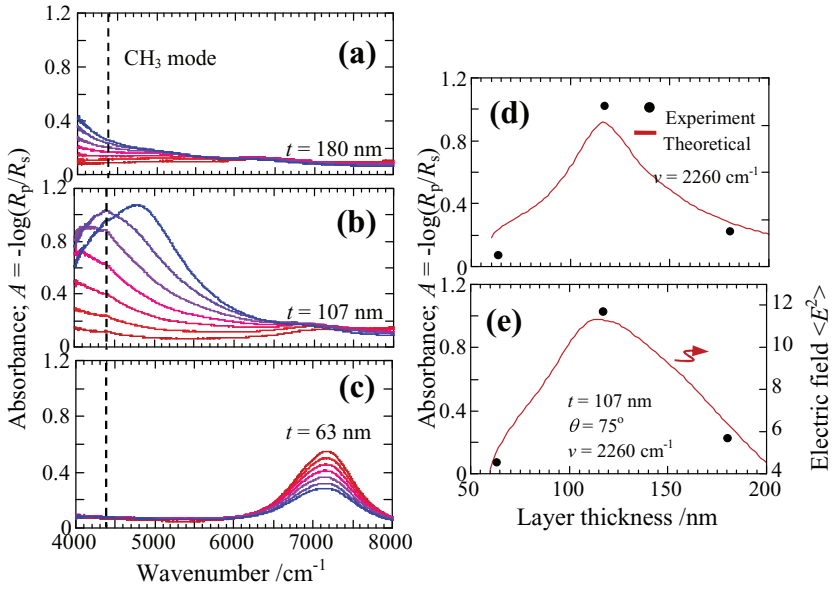

Figure 4. SPR-NIR spectra of In_2O_3:Sn layers with thicknesses of 180 nm (a), 107 nm (b), and 63 nm (c). Methanol (CH_3OH) was chosen as the dielectric medium. The incident angle (θ) varies from 64 degrees (red line) to 76 degrees (blue line) in 2-degree increments. The black dotted lines represent the absorption band (CH_3 mode) of water.

component, $\langle E_{\perp}^2 \rangle$, and its projections in two orthogonal directions, $\langle E_{zz}^2 \rangle$ and $\langle E_{xz}^2 \rangle$, as a function of depth (z). The direction x is parallel to the surface of the layers. The direction of depth is normal to the layer, and the intensities of the mean-square electromagnetic fields are normalized to that of the incident radiation. The calculation was carried out as a function of layer thickness under conditions involving an incident angle of θ = 75 degrees and a wavenumber of 5173 cm^{-1}. In the case of a multilayer (BK-7–In_2O_3:Sn–water) corresponding to the geometry of the SPR system, the electromagnetic field amplitude at the In_2O_3:Sn–water interface was clearly enhanced by SPR compared with ATR (Figure 3a,b). The increase of water absorbance was associated with that of the electromagnetic field amplitude as a function of layer thickness (Figure 3c). It was revealed that the enhancement of water absorbance was attributed to SPR excited on an In_2O_3:Sn layer surface as a consequence of the coupling between plasmon and vibration excitations in the NIR range.

A similar situation was also observed when using methanol media with a vibrational mode ascribed to CH_3 (4424 cm^{-1}) due to the combination of CH_3 stretching and bending modes.[25] A 107 nm-thick layer showed an SPR spectrum with the CH mode in the range 5000 to 4000 cm^{-1} when the peak position of absorption of methanol overlapped with that of SPR (**Figure 4**a–d). Strong electromagnetic field amplitude $<E^2>$ induced on In_2O_3:Sn surfaces clearly enhanced the absorption of the CH_3 mode (Figure 4e). These findings suggested the same mechanism as the enhancement of water absorption, which supported the results of coupling between a surface plasmon and molecular vibrations. Therefore, absorption-sensitive SPR was demonstrated for the first time using doped oxide semiconductors. The water and methanol absorption in relation to OH and CH_3 modes caused a slight change of the refractive index (n) in the order of 10^{-4} (Figures S5a and S7b], which indicted that oxide-based SPR can at least detect changes of the refractive index in the order of $\Delta n/n \sim 10^{-4}$ in the NIR range, which is closely related to the detection sensitivity.

4. Detection Sensitivity of Oxide-Based SPR

We then estimated the exact detection sensitivity of oxide-based SPR by sensing the refractive index using SPR measurements of different glucose concentrations in water. In the infrared range 4000 to 1000 cm^{-1}, the absorption of water is higher than that of glucose, and is inefficient for the measurement of glucose in water.[26,27] However, the large difference in the real part of the refractive indices between glucose and water components exists in the NIR range 5000 to 4000 cm^{-1} (Figure S6a). Accordingly, the sensing ability of oxide-based SPR in the NIR range can be estimated from experimental and theoretical viewpoints in the following manner.

Figure 5a shows SPR spectra at θ = 75 degrees for water solutions with different glucose concentrations from 1 to 10 g/dL. The vertical axis is expressed as $A = -\log (R_p / R_s)$. An In_2O_3:Sn layer with a thickness of 107 nm was chosen for SPR measurement. The SPR peak gradually shifted to lower wavenumbers with the glucose concentration. We also observed a small wavenumber shift of 4.82 cm^{-1} with a low glucose concentration of 100 mg/dL (Figure 5b). The peak shift of SPR ($\Delta\nu$) was linearly correlated with the glucose concentration (Figure 5c), revealing that oxide-based SPR possesses sufficient functionality as a sensing device. $\Delta\nu$ is defined as the differential wavenumber between SPR peaks of water and water-glucose solutions. The RIU (refractive index unit) corresponding to a glucose concentration of 100 mg/dL was 2.9×10^5 at 2134 nm (4686 cm^{-1}) for a wavelength shift resolution of 0.07 nm (1 cm^{-1}). The change of the refractive index of a glucose-water solution was 10^{-5} at a glucose concentration of 100 mg/dL in water (Figure S6). Figure 5c shows that the detection limit of oxide-SPR was 29.3 cm^{-1}/(g/dL) (7576 nm RIU^{-1}), which was similar to that of the theoretical estimation based on Fresnel equations (17.7 cm^{-1}/(g/dL); 7447 nm RIU^{-1}). The detection limit of oxide-based SPR was close to that of Au metal-based SPR in the visible range. The detection sensitivity of Au metal-based SPR was 970 and 13 800 nm RIU^{-1} at wavelengths of 630 and 850 nm, respectively (**Table 2**).[28] This is related to spatial coherence of an SP wave on a metal surface, which will be discussed later. For an additional understanding of the detection sensitivity, we estimated the figure of merit (FoM) of oxide-based SPR in the NIR region from Figure 5. The sensing performance of surface plasmon resonance can be characterized by considering the relation $FoM = S_{bulk}/\Delta\lambda$, where $\Delta\lambda$ is the resonace width (full width at half-maximum) and S_{bulk} is the bulk sensitivity defined as $S_{bulk} = \partial\lambda/\partial n$. This equation indicates the shift of the resonance wavelength with a change

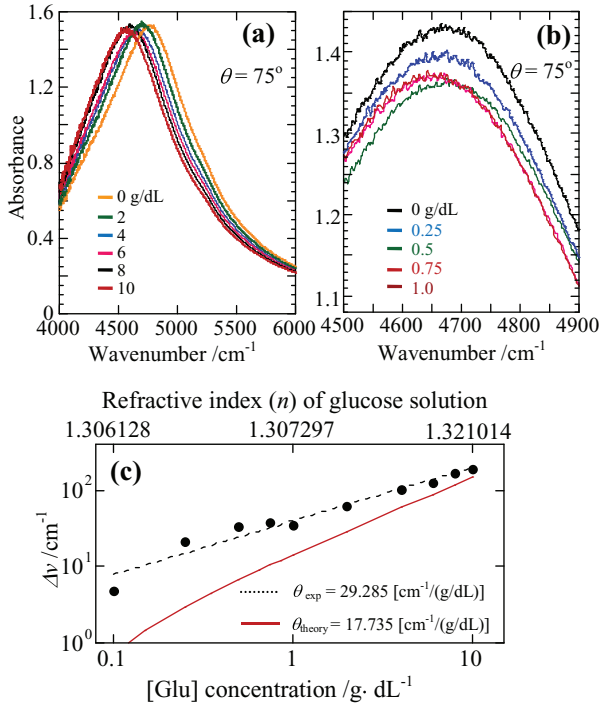

Figure 5. SPR spectra obtained using glucose-water solutions comprising high glucose concentrations from 0 to 10 g/dL with increments of 2 g/dL (a), or low glucose concentrations from 0 to 1 g/dL with increments of 0.25 g/dL (b). All SPR spectral measurements were performed with θ = 70 degrees. Relationship between the wavenumber shift of SPR ($\Delta\nu$) and glucose concentration. The change of refractive index in a glucose-water solution is also expressed in the upper horizontal axis. The dotted line represents a visual guide of the experimental data, while the solid line indicates the relationship obtained from theoretical calculations.

of the refractive index of the surrounding*n*. The experimentally obtained FoM was 13.5, which is close to the thoretical value of 12.6 at the same wavelength. We demonstrated a large FoM for oxide-SPR of more than 1 order of magnitude in the NIR region.

5. Spatial Sensing Regions of Oxide-Based SPR in the NIR Range

Spatially sensing regions of the SP can be described by the propagation length (L_{sp}) on a layer surface, and the penetration depth (δ_w) into water [See Section 9 of the Supporting Information].[29] **Figure 6**a shows that the wavenumber-dependent propagation length of the SP was within several

Table 2. Detection sensitivity in oxide- and Au metal-based SPR.

Metal layer supporting SPW	In_2O_3:Sn	Au	
Wavelength (λ) [nm]	2200	630	850
Frequency (v) [cm^{-1}]	4545	15 337	11 764
Sensitivity [nm RIU^{-1}]	7576	970	13 800
Resolution [RIU]	2.9×10^{-5}	2.0×10^{-5}	1.0×10^{-6}

[a]Sensitivity and resolution of Au were taken from Ref. [28].

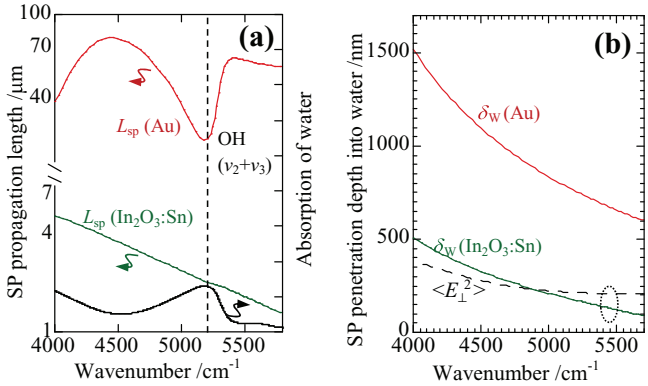

Figure 6. (a) Propagation length (L_{sp}) of SP waves on In_2O_3:Sn and Au layers as a function of wavenumber. (b) Penetration depth (δ_w) of SP waves on In_2O_3:Sn and Au layers as a function of wavenumber. The dotted line represents the penetration depth at which the electromagnetic field $\langle E_\perp^2 \rangle$ fell to $1/e$ at the same wavenumbers.

micrometers and was influenced slightly by plasmon damping from the water absorption at 5173 cm^{-1}. We also confirmed the plasmon damping of the propagation length of the SP into methanol media caused by CH absorption (Figure S7). It was shown that the coupling between a surface plasmon and vibrational excitation resulted in the appearance of an absorption peak ascribed to water in SPR spectra. The value of L_{sp} for oxide-based SPR was similar to that of Au metal-based SPR in the visible range (L_{sp} = 2.64 μm at λ = 652 nm, **Table 3**). On the other hand, the wavenumber-dependent penetration depth was in the range δ_w = 0.15 to 0.4 μm in the SPR of the In_2O_3:Sn–water interface (Figure 6b), which was close to the penetration depth at which the electromagnetic $\langle E_\perp^2 \rangle$ field fell to $1/e$ for the same wavenumbers (dotted lines in Figure 6b). The enhanced absorption of water and glucose detection in the NIR range was due to a change of the refractive index within several hundred nanometers from the In_2O_3:Sn layer surface.

The above results revealed that spatial sensing regions of oxide-based SPR were smaller than those of Au metal-based SPR having longer δ_w values exceeding 1 μm in the NIR range. However, Au metal-based SPR in the visible range becomes exceedingly small: δ_w < 0.2 μm (Table 3). The values of δ_w in oxide-based SPR were similar to those of Au metal-based SPR in the visible range, which was consistent with the fact that oxide-based SPR showed the same detection sensitivity in the order of 10^{-5} RIU as Au metal-based SPR in the visible range. Moreover, the penetration depth of the electromagnetic field amplitude in terms of In_2O_3:Sn and Au layers showed a similar behavior (Figure S8a,b). These results confirmed by the surface plasmon properties of conductor loss (k_{sp}") and field concentration into media of an SP wave at the metal-media interface (Table 3). Accordingly, the detection sensitivity and spatial sensing regions of Au metal-based SPR in the visible range were realized in the NIR range when using oxide-based SPR. This resulted from a red-shift of plasmon frequency following the decrease of electron density in the host. It is known that Au metal-based SPR in the visible range plays an important role in the detection of biological and chemical reactions at the nanoscale. Therefore,

Table 3. Major characteristics of surface plasmon waves (SPW) at the metal–water interface.[a–c)]

Metal layer supporting SPW	In_2O_3:Sn	Au	
Wavelength (λ) [nm]	2200	652	2200
Frequency (v) [cm^{-1}]	4545	15 337	4545
Conductor loss of SPW, $k_{SP}'' = (\varepsilon''/(\varepsilon')^2)$	3.20×10^{-2}	1.07×10^{-2}	7.65×10^{-4}
Propagation length, L_{sp} [μm]	3.51	2.64	74.7
Penetration depth into water, δ_w [μm]	0.473	0.168	1.07
Penetration depth into metal, δ_m [μm]	0.116	0.030	0.025
Field concentration in water media [%]	80.3	84.8	97.7
Complex dielectric constants ($\varepsilon = \varepsilon' + i\varepsilon''$)	−6.87 + 1.507i	−9.89 + 1.05i	−188 + 27.1i

[a)]Optical constants of Au were taken from Ref. [30]; [b)]Optical constants of water were taken from Ref. [31]; c)Optical constants of In_2O_3:Sn were taken from Figure S2a.

unlike the case with Au metal-based SPR, it is expected that surface sensing in the order of several hundred nanometers can be used with oxide-based SPR in the NIR range, which can be combined with molecular vibrational spectroscopy. SPR devices utilizing In_2O_3:Sn may be explored to optically detect immunoanalytes and investigate their use in combination with electrochemical measurements. This work has shown that SPR on doped oxide semiconductors can be employed in practical situations for use in surface sensing applications at the nano scale in the NIR range. Although there are advantages of oxide-based SPR with In_2O_3:Sn, the surface chemistry makes it difficult to tailor the material when considering applications in biosensing. The layer surfaces of In_2O_3:Sn are terminated by InOOH and $In(OH)_3$-like species due to exposure to water vapor after layer deposition, which induces chemical instability of In_2O_3:Sn layer surfaces.[32] In order to obtain chemically stabilized In_2O_3:Sn layer surfaces, it may be advantageous to apply weak carboxylic acid linkages, siloxane or phosphonate linkages with varying stability in different pH ranges.[33–35] These surface modification techniques will take advantage of the inherent In_2O_3:Sn-based SPR properties for biosensors or cell biological studies.

6. Conclusion

We investigated the detection sensitivity of oxide-SPR using an oxide semiconductor of In_2O_3:Sn. SPR phenomena were clearly observed in the NIR range at layer thicknesses above 107 nm. An obvious enhancement of the absorption bands in relation to water and methanol media was confirmed when the absorption peak of OH in water (CH in methanol) and the SPR peak overlapped. These enhancement effects played an important role in increasing the evanescent field amplitudes at the interfaces of In_2O_3:Sn/dielectric media (water and methanol). Moreover, SPR measurements with glucose-water solutions were carried out in order to determine the detection sensitivity of oxide-SPR. The sensitivity of the refractive index of SPR using an In_2O_3:Sn layer was determined as 29.3 $cm^{-1}/(g/dL)$ (7576 nm RIU^{-1}) with a wavelength resolution of 0.07 nm. This sensitivity was greater than that of the detection ability of Au metal-based SPR in the visible range, and is discussed in regard to the spatial coherence of SP and evanescent waves.

7. Experimental Section

Film Deposition: $In_{2-x}Sn_xO_3$ layers (x = 0.20) were fabricated by a pulsed laser deposition (PLD) method. The optimized growth temperature and partial oxygen pressure were 500 °C and 10^{-3} Pa, respectively. The beam out of an ArF excimer laser (193 nm and 1 J/cm^2) was focused on an In_2O_3:Sn ceramic target (99.99%) at a repetition of 10 Hz. The film thickness was varied within the range 63 to 180 nm. A glass substrate (BK-7) with a refractive index of 1.517 was chosen in order to use an attenuated total reflection (ATR) system with a BK-7 prism. Atomic force microscopy revealed a root-mean-square roughness of 2 nm, which was so smooth that the effect of localized surface plasmons was negligibly small in the NIR region. Hall measurements revealed that the electron density of layers was in the order of 0.8 to 2×10^{21} cm^{-3}, which indicated that the real part of the complex dielectric constants possessed negative values in the NIR range. Typical structural quality and optical properties of the layers are reported in the Supporting Information (Figures S1 and S2).

Spectral Measurements: Surface plasmon resonance (SPR) excitation was carried out using a Kretschmann-type ATR, except for the presence of metallic oxide film on the surface for internal reflection. At each incident angle, 16 scans were co-added at a band-pass filter of 4 cm^{-1} by a Fourier-transform near-infrared (FT-IR) spectrometer (Bruker, Vector 22/N), which was connected to the SPR attachment with fiber optics. The substrate deposited with an In_2O_3:Sn film was placed on the prism with index matching fluid (polyethylene glycol). The light beam from the external port of the FT-NIR spectrometer is sent through quartz fiber optic to a planoconvex lens, which focuses the beam on a slit. The beam is collimated in a BK-7 hemicylinder prism to a beam width of 1 nm, and the size of the beam spot onto the reflective surface is less than 2 mm^2. Details of the apparatus have been described elsewhere.[7] SPR measurements were taken at different incident angles (θ) in the range 61.0 to 75.0°. The spectral intensity of measurements was recorded as an absorbance ratio [$A = -\log (R_p / R_s)$] in the wavenumber (ν) range 8000 to 4000 cm^{-1}, where R_p and R_s denote the *p*- and *s*-polarized reflection light, respectively.

Supporting Information

Supporting Information is available from the Wiley Online Library or from the author.

Acknowledgements

The authors acknowledge Dr. Noriyuki Hasuike and Prof. Hiroshi Harima from the Kyoto Institute of Technology (Japan) for assistance with the fundamental optical properties of In_2O_3:Sn layers. Support for this work was provided in part by a Grand-in-Aid for Young Scientists from the Japan Society for the Promotion of Science, and a research grant from the Toyota Physical and Chemical Research Institute.

Received: December 29, 2012
Revised: March 1, 2013
Published online: May 3, 2013

[1] K. Manthiram, A. P. Alivisatos, *J. Am. Chem. Soc.* **2012**, *134*, 3995.
[2] G. Garcia, R. Buonsanti, E. L. Runnerstrom, R. J. Mendelsberg, A. Llordes, A. Anders, T. J. Richardson, D. J. Milliron, *Nano Lett.* **2011**, *11*, 4415.

[3] W. Badalawa, H. Matsui, A. Ikehata, H. Tabata, *Appl. Phys. Lett.* **2011**, *99*, 011913.
[4] B. Liedberg, C. Nylander, I. Lunström, *Sens. Actuators* **1983**, *4*, 299.
[5] J. Homola, S. S. Yee, G. Gauglitz, *Sens. Actuators B* **1999**, *54*, 3.
[6] A. Ikehata, T. Itoh, Y. Ozaki, *Anal. Chem.* **2004**, *76*, 6461.
[7] A. Ikehata, K. Ohara, H. Shinzawa, Y. Ozaki, *Appl. Spectrosc.* **2008**, *5*, 517.
[8] F. Neubrech, A. Pucci, T. W. Cornelius, S. Karim, A. Garciá-Etxarri, J. Aizpurua, *Phys. Rev. Lett.* **2008**, *101*, 157403.
[9] W. Kaye, *Spectrochimia Acta* **1954**, *6*, 25.
[10] *Near-infrared Spectroscopy Principles, Instruments, Applications* (Eds: H. W. Siesler, Y. Ozaki, S. Kawata, H. M. Heise), Wiley-VCH, Weinheim, Germany **2002**.
[11] C. Pasquini, *J. Braz. Chem. Soc.* **2003**,*14*,198.
[12] H. Ohta, M. Orita, M. Hirano, H. Tanji, H. Kawazoe, H. Hosono, *Appl. Phys. Lett.* **2000**, *76*, 2740.
[13] T. Yamada, H. Makino, N. Yamamoto, T. Yamamoto, *J. Appl. Phys.* **2010**, *107*, 123534.
[14] D. Ruzmetov, D. Heiman, B. B. Claflin, V. Narayanamurti, S. Ramanathan, *Phys. Rev. B* **2009**, *79*, 153107.
[15] H. Tang, K. Prasad, R. Sanjinès, P. E. Schmid, F. Lévy, *J. Appl. Phys.* **1994**, *75*, 2042.
[16] D. B. Migas, V. L. Shaposhnikov, V. E. Borisenko, *J. Appl. Phys.* **2010**, *108*, 093714.
[17] A. N. Asanov, W. W. Wilson, P. B. Oldham, *Anal. Chem.* **1998**, *70*, 1156.
[18] X. H. Yang, Q. Wang, K. M. Wang, W. H. Tan, J. Yao, H. M. Li, *Langmuir* **2006**, *22*, 5654.
[19] W. Luo, N. P. Westcott, A. Pulsipher, M. N. Yousaf, *Langmuir* **2008**, *24*, 13096.
[20] M. Klis, M. Karbarz, Z. Stojek, J. Rogalski, R. Bilewicz, *J. Phys. Chem.* **2009**, *113*, 6062.
[21] T. K. Tam, M. Pita, O. Trontsenko, M. Motornov, I. Tokarev, J. Halámek, D. Minko, E. Katz, *Langmuir* **2010**, *26*, 4506.
[22] J. L. Debéthune, *Surf. Sci.* **1979**, *82*, 461.
[23] H. Kano, S. Kawata, *Appl. Optic.* **1994**, *33*, 5166.
[24] S. Ekgaist, C. Thammacharon, W. Knoll, *Anal. Chem.* **2004**, *76*, 2210.
[25] R. Iwamoto, A. Nara, T. Matsuda, *Appl. Spectrosc.* **2006**, *60*, 450.
[26] E. D. Park, *Handbook of Optical Constants of solids*, Academic Press, New York **1991**.
[27] M. Jetzki, R. Signorell, *J. Chem. Phys.* **2002**, *117*, 8063.
[28] J. Homola, S. S. Yee, G. Gauglitz, *Sens. Actuators* **1999**, *54*, 3.
[29] H. Raether, *Surface Plasmons on Smooth and Rough Surfaces and Gratings*, Springer, Berlin **1998**.
[30] I. Thormahlen, J. Straub, U. J. Grigull, *J. Phys. Chem. Ref. Dat.* **1985**, *14*, 933.
[31] P. B. Johnson, R. W. Christy, *Phys. Rev.* **1972**, *6*, 4370.
[32] J. S. Kim, P. K. H. Ho, D. S. Thomas, R. H. Friend, F. Cacialli, G.-W. Bao, S. F. Li, *Chem. Phys. Lett.* **1999**, *315*, 307.
[33] M. S. Kang, H. Ma, H. L. Yip, A. K.-Y. Jen, *J. Mater. Chem.* **2007**, *17*, 3489.
[34] S. F. J. Appleyard, S. R. Day, R. D. Pickford, M. R. Willis, *J. Mater. Chem.* **2000**, *10*, 169.
[35] E. L. Hanson, J. Guo, N. Koch, J. Schwartz, S. L. Bernasek, *J. Am. Chem. Soc.* **2005**, *127*, 10058.